Transactions of the Korean Nuclear Society Spring Meeting
Jeju, Korea, May 23-24, 2019

Prediction of Steam Generator Tube Gap Velocities during Feedwater Blowdown

Jong Chull Jo [a,b*], Jae Jun Jeong [a], Byong-Jo Yun [a], Jongkap Kim [b], Frederick J. Moody [c]
[a]*Pusan National University, School of Mechanical Engineering, Geumjeong-gu, Busan, 46241, Korea*
[b]*Korea Institute of Nuclear Safety, Reactor System Evaluation Dept., Yusung-gu, Daejon, 34142, Korea*
[c] *2125 N. Olive Ave. APT D 33, Turlock, CA, 95382-1936, USA*
[*]*Corresponding author: jongcjo@pusan.ac.kr; jcjo@kins.re.kr*

1. Introduction

Tubes of steam generators (SGs) at pressurized water reactors (PWRs) pant can be subjected to flow-induced vibration (FIV) during normal operation as well as abnormal operation following a main steam line or feedwater line break (FWLB) accident. The FIV mechanisms includes turbulence excitation, vortex-shedding, fluidelastic instability, and acoustic resonance [1]. Among them, the fluidelastic instability has been addressed as the most important potential damage mechanism for the SG tubes because it caused several SG tube rupture events at PWR nuclear power plants worldwide in the past. The fluidelastic instability of the tube occurs when any tube being subjected to the tube-to-tube gap cross-flow velocity exceeds a threshold value named critical velocity. If the gap velocity increases beyond the threshold value, the tube begins to vibrate with steeply increasing amplitude since the whole energy absorbed by the tube from the external fluid flow exceeds the energy that the tube dissipates to the environment by the amplitude-limited vibration. This fluidelastic instability results in serious mechanical damages on the tube such as fretting-wear, impact-collision, and high-cycle fatigue leading to tube rupture in a short term. In the process of the structural integrity evaluation of PWR SG tubes being subjected to FIV and/or transient hydraulic loading, one of the key prerequisites is to predict the tube-to-tube gap velocity distributions along the tubes which are most susceptible to the fluidelastic instability. This paper presents two different approaches to predict the tube-to-tube gap velocity distributions during sub-cooled feedwater (FW) blowdown caused by a FWLB using CFD calculations.

2. Analysis Models for CFD Calculation of SG Secondary Side Flow Field

2.1 Problem

The objective of this study is to present two different approaches to estimate the tube-to-tube gap velocity distributions during subcooled FW blowdown using the CFD calculations. One is to directly calculate the velocity distributions by simulating the secondary side flow fields of a realistically simplified SG model containing tubes. The other is to indirectly predict those by using the CFD calculation results for a tubeless SG model and the porosity of the SG model with tubes. The latter approach is easier to implement than the former because of the simplicity of the SG model.

As in the previous works [2-4], the FW blowdown is assumed to be caused by a FWLB. The break is defined to occur in a moment during the SG full power operation or hot standby modes at a weld point on the FW line so that the pressure at the cross-section of the broken pipe end drops instantaneously. In addition, upon receipt of the FWLB signal, the SG main steam line is assumed to be blocked. When the FW pipe breaks abruptly at a weld point, the FW flow into the SG will be interrupted and then the water will begin to flow out from the SG through the broken pipe end. Therefore, the initial velocity $U_i = 0.0\ \mathrm{m/s}$ is assumed. It is assumed that the SG secondary side fluid temperature increases from the FW inlet temperature of 232 ℃ at the SG bottom to the saturation temperature at 7.5 MPa (290.54 ℃) in the upper steam space.

2.2 SG Analysis Model

The SG analysis model considered in this study is shown in Fig. 1. It contains 30 vertical straight tubes and has a porosity $\varepsilon = 0.56$.

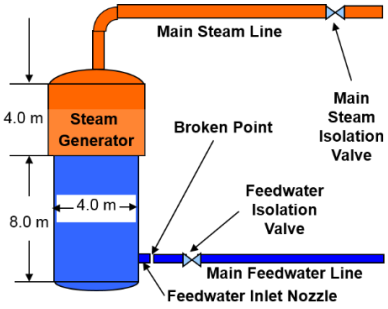

Fig.1 Simplified FWLB analysis model [2-4]

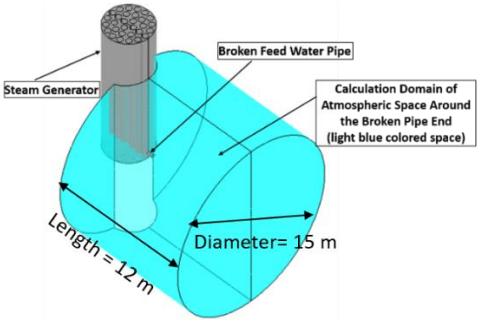

Fig. 2 Calculation domain of the subcooled water flashing flow analysis model

For this simplified SG model, transient hydraulic responses of the secondary side flow fields to a FWLB have been numerically analyzed by applying three

different blowdown discharge flow models such as the subcooled non-flashing water flow model, the saturated water flashing flow model, and the subcooled water flashing flow model [1-3]. The calculation domain of the present analysis model is displayed in Figure 2. This calculation domain covers the SG inside, the nozzle section of the broken FW pipe, and the atmospheric space surrounding the broken pipe end. The constant atmospheric pressure are assumed to maintain at the outer boundaries of the calculation domain for the surrounding atmospheric space being occupied initially by still air at 25 ℃ and 1 atm during blowdown.

2.3 Numerical Model

The mathematical formulation of the analysis model is the same as in reference [3]. The inhomogeneous two-fluid model is used to calculate the subcooled water flashing flow. The $k-\omega$ based SST model [5] is applied for estimating the turbulent viscosity. The conservation equations are solved by closing with a relation among pressure, molecular volume and temperature of the fluid by using a commercial CFD code [6]. The thermal phase change model is applied to predict the heat and mass transfer between liquid and vapor phases.

2.3 Numerical Analysis

Time integration is proceeded by the fully implicit second order backward Euler method using automatically adjusted time steps ranging between 0.001 ms and 0.01 ms to meet the Courant-Friedrichs-Lewy criterion [6]. For each time step, the computation iterations are set to terminate if the maximum of the absolute sum of dimensionless residuals of the governing equations is less than 0.0001. The boundary conditions at all of the solid wall surfaces are specified to be adiabatic and no-slip. The transient fluid velocity and pressure in the SG secondary side are monitored at six different locations "P1 ~ P5" and the exit section as shown in Fig. 3.

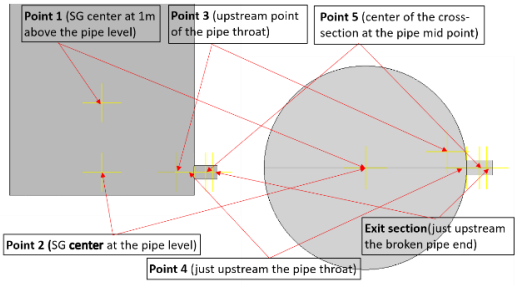

Fig.3 Monitoring points

Area averaged values of the fluid velocity are monitored at the exit cross-section just upstream the pipe end. The discretization of the calculation domain is made as fine as reasonably practicable.

3. CFD Calculation Results and Discussion

3.1 Numerical Simulation of Subcooled Flashing Flow

Figures 4 and 5 show the typical results of the CFD calculations using the subcooled water flashing flow model for the no tubed SG model in terms of the static pressure and void fraction contours.

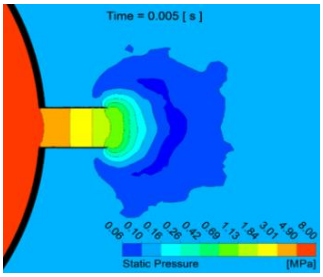

Fig.4 Static pressure contour

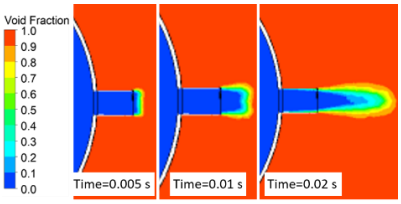

Fig.5 Void fraction contours

From Figs. 4 and 5, it is seen that, in the early time period of blowdown following a FWLB, the flashing flow core maintains a metastable state due to rapid passing of the discharging fluid through the broken pipe without forming any critical flow situation. This is because the highly compressed subcooled water being discharged through the broken pipe can hardly change its phase in a very short time.

Figure 6 shows the transient streamlines in the 30 tubed SG secondary flow field during blowdown.

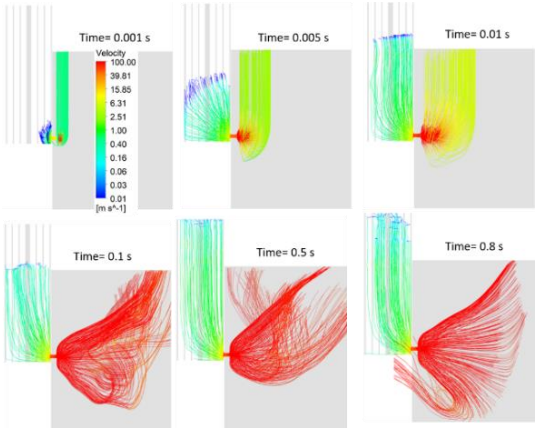

Fig.6 Streamlines during blowdown

3.2 Tube-to-Tube Gap Velocities Calculated Using the Two Different SG Models

The CFD calculation results of the transient responses of the fluid velocity in the SG secondary side to the FWLB for two different SG models are shown in Fig. 7. One is the hollow SG model which contains no tubes and the other is the tubed SG model which contains 30 tubes. When the tubed SG model is simulated, the transient SG tube-to-tube gap velocities and pressures can be predicted directly. In addition, those can be also estimated from the calculation of flow field for the hollow SG model (containing no tubes) by using the following simple relation.

$$V_{g,avg} = V_\infty/\varepsilon \quad (1)$$

where $V_{g,avg}$ and V_∞ are the average tube-to-tube gap fluid velocity in the SG model containing tubes and the fluid velocity in the hollow SG model, respectively.

As can be seen from Fig. 7, the transient tube-to-tube gap fluid velocities at the monitoring point1 1, 2, 3 and 4 in the SG model containing 30 tubes (where $p = 0.8\,m$, $d = 0.6\,m$) are approximately equal to the estimations from the calculation of flow field for the hollow SG model using Eq.(1). Both SG models yield little differences in the fluid velocities inside the FW pipe.

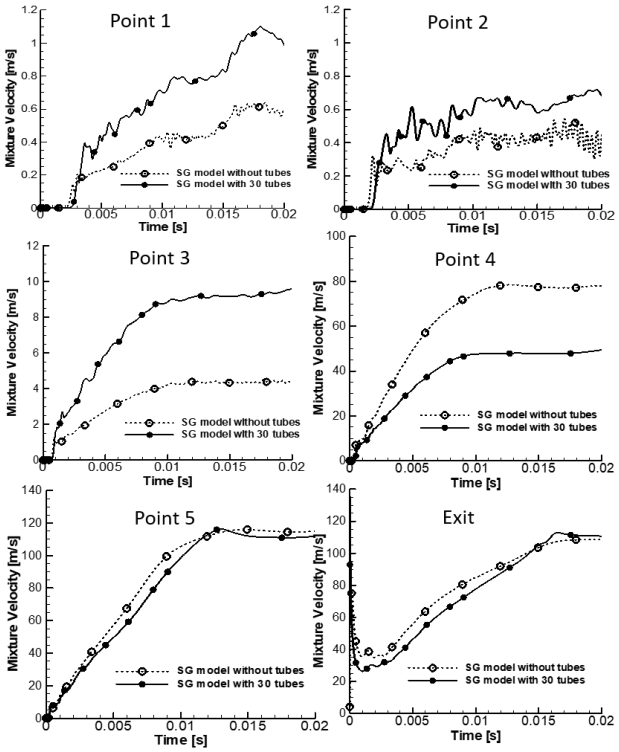

Fig.7 Comparison of the mixture velocities at the monitoring points between the two different SG models

3.3 Analytical Approximation of the SG flow fields

Although experimental data may be the subject of future studies by research groups, another way of validating CFD studies, like those predicting complex flow fields, is to use supportive, independent analyses that do not employ the same predictive methods as the CFD approach, and compare the calculated results. That approach is applied in this study. The volume flow rate of water, Q, entering the broken FW line creates velocity and pressure fields inside the SG. Point P4 inside the SG is several centimeters in front of the FW line entrance, and point P5 is inside the FW line half way to the exit where non-flashing water is flowing in this region. The water velocity just inside the FW line entrance is interpolated between points P4 and P5 in Fig. 7 as $V \approx 93$ m/s. Since the FW line diameter is d_{pipe} = 0.3 m with an area of A_{pipe} = 0.07 m^2, the water volume discharge flow rate must be approximately $Q = A_{pipe}V = 6.51\,m^3/s$, which will be used in the simplified model for predicting the SG velocity and pressure fields. Rather than attempt to include several thousand tubes that exist in the SG, the CFD model was developed using 30 large tubes of diameter $d = 0.6\,m$, spaced vertically to obtain the same porosity, $\varepsilon = 0.56$ as the actual SG.

The simplified model described in this review is based on two-dimensional flow in the x, y plane, bounded by a vertical rectangle with a horizontal base and vertical left and right sides, with a point sink on the right side simulating the discharge line as shown in Fig. 8. The cylindrical SG of diameter $D = 4.0\,m$ and cross-sectional area $A_{SG} = \frac{\pi D^2}{4} = 12.57\,m^2$ actually is simulated by a vertical rectangular parallelepiped with a square base of side $L = 3.54\,m$, which has the same cross-sectional area as the cylinder. The front face of the rectangle is in the x, y plane and the adjacent parallel sides extend backward in the z direction to the rear face, which is parallel to the x, y plane. The water height in both the cylinder and rectangle is $H = 8.0\,m$.

Darcy's equation [7, 8] for flow in porous media was first employed to relate fluid velocity, pressure, and gravity in terms of the media permeability (which includes porosity) and viscosity (if the flow is laminar). For incompressible liquid, continuity shows that the velocity field can be described with a velocity potential that satisfies Laplace's equation, and therefore can be treated as the real component of the complex velocity potential. A specific mapping in the literature [9] is employed to predict an approximate flow field in the vertical rectangle with a volume discharge rate from the point sink on the right side. For the rectangular geometry in the x, y plane, the point sink is the end view of a line sink in the z coordinate of length $L = 3.54\,m$, for which the volume flow rate per unit length is given by $Q' = \frac{Q}{L} = \frac{6.51}{3.54} = 1.84\,m^3/s$. Several pressure and velocity profiles are calculated and values predicted by the CFD method are compared with the results.

A model cylinder is considered with internal tubes that are homogenized to make the internal porosity ε identical to the actual SG. A single point sink in the side of the cylinder to simulate the feedwater line discharge leads to a mathematical problem almost as difficult as the CFD simulation employed. However, if the cylindrical SG is roughly formed as a rectangular box with a square base and the feedwater discharge is simulated as a line sink as shown in Fig. 8, an approximation of the flow field is possible.

The SG internals are homogenized as a porous medium in Fig. 1 with a void fraction or porosity $\varepsilon = 0.56$. The base of the square has area L^2, which is set equal to the SG cylindrical area $\pi D^2/4$, or $L = D\sqrt{\pi}/2$. For the SG with diameter $D = 4.0\,m$, the length $L = 3.54\,m$. The water height $H = 8.0\,m$ and feedwater line height $h = 1.0\,m$ remain the same for both the cylinder and rectangle.

The velocity field in porous media is governed by Darcy's Law [7, 8],

$$\boldsymbol{V} = -\frac{\zeta}{\mu}(\nabla P - \mathbf{j}\rho g) \quad (2)$$

where ζ and μ are the permeability and dynamic viscosity, respectively.

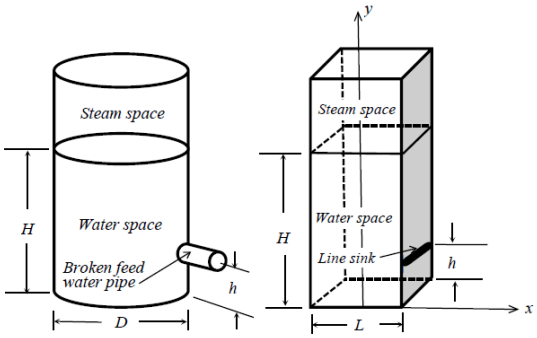

Fig. 8 SG—equivalent rectangular shape

Equation (2) states that the local fluid velocity vector is proportional to the local pressure gradient minus the hydrostatic pressure gradient.

The velocity is given in terms of a velocity potential ϕ,

$$\boldsymbol{V} = \nabla\phi \tag{3}$$

For incompressible liquid, the continuity or mass conservation (Laplace's) equation is

$$\nabla \cdot \boldsymbol{V} = \nabla \cdot \nabla\phi = \nabla^2\phi = 0 \tag{4}$$

A two-dimensional flow field in the x, y plane for the rectangular geometry of Fig. 8 lends itself to available conformal maps from complex variable theory. Velocity $\boldsymbol{V}$ and its x and y components u and v correspond to flow in the region as if it were unobstructed. For the two-dimensional geometry, which simulates a potential flow in a rectangular region with a point sink on the right side at elevation $y = h$ (actually the line sink in the z coordinate), the velocity potential ϕ is obtained from the complex potential function Φ, which can be expressed as a function of the complex variable $z\ (= x + iy)$[9].

$$\Phi(z) = \phi + i\psi = -\frac{Q'}{\pi}\ln\left(\sin\frac{\pi z}{L} - \cosh\frac{\pi h}{L}\right) \tag{5}$$

Where ψ is the stream function and Q' is the volume discharge rate per unit length of the line sink extending into the page length L as shown in Fig. 8. The horizontal and vertical velocity components u and v are obtained by first writing

$$\frac{d\Phi}{dz} = u - iv = -\frac{Q'}{L}\frac{\cos\frac{\pi z}{L}}{\sin\frac{\pi z}{L} - \cosh\frac{\pi h}{L}}$$

$$= -\frac{Q'}{L}\frac{\left(\cos\frac{\pi x}{L}\cosh\frac{\pi y}{L} - i\sin\frac{\pi x}{L}\sinh\frac{\pi y}{L}\right)}{\left(\sin\frac{\pi x}{L}\cosh\frac{\pi y}{L} - \cosh\frac{\pi h}{L}\right) + i\cos\frac{\pi x}{L}\sinh\frac{\pi y}{L}} \tag{6}$$

Multiplying the numerator and denominator by the complex conjugate of the denominator leads to the real (not imaginary) velocity components,

$$u(x,y) = -\frac{Q'}{L}\frac{\cos\frac{\pi x}{L}\left(\sin\frac{\pi x}{L} - \cosh\frac{\pi y}{L}\cosh\frac{\pi h}{L}\right)}{\left(\sin\frac{\pi x}{L}\cosh\frac{\pi y}{L} - \cosh\frac{\pi h}{L}\right)^2 + \left(\cos\frac{\pi x}{L}\sinh\frac{\pi y}{L}\right)^2} \tag{7}$$

$$v(x,y) = -\frac{Q'}{L}\frac{\sinh\frac{\pi y}{L}\left(\cosh\frac{\pi y}{L} - \sin\frac{\pi x}{L}\cosh\frac{\pi h}{L}\right)}{\left(\sin\frac{\pi x}{L}\cosh\frac{\pi y}{L} - \cosh\frac{\pi h}{L}\right)^2 + \left(\cos\frac{\pi x}{L}\sinh\frac{\pi y}{L}\right)^2} \tag{8}$$

The horizontal velocity component u dominates at the broken feedwater elevation $y = h = 1.0\,m$. Employing $Q' = 1.84\,m^3/s$ and $L = 3.54\,m$, and for a horizontal range from the left wall at $x = -$ 1.77 m to the right wall approaching $x = +$ 1.77 m, $u(x,h)$ from Eq. (7) is

$$u(x,h) = -\frac{Q'}{L}\frac{\cos\frac{\pi x}{L}\left(\sin\frac{\pi x}{L} - \cosh^2\frac{\pi h}{L}\right)}{\cosh^2\frac{\pi h}{L}\left(\sin\frac{\pi x}{L} - 1\right)^2 + \cos^2\frac{\pi x}{L}\sinh^2\frac{\pi h}{L}} \tag{9}$$

, which is shown in Fig. 9. The solid black line is from Eq. (9). The points labeled P2 and P3 are predictions from the CFD calculation. As *x* approaches the right wall and the discharging FW line, the model velocity approaches a singularity and the solution is undefined, but close predictions are noted for the two CFD locations shown. A close prediction also was obtained for point P1 on the centerline above P2 although it is not shown.

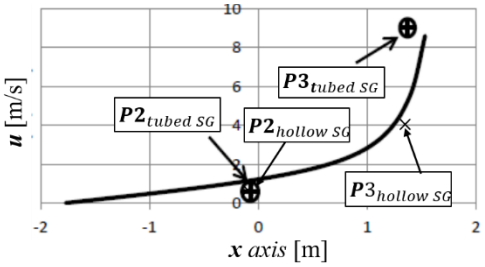

Fig.9 Comparison of the horizontal velocities at the FW line elevation, $y = 1.0\,m$ between CFD calculation and analytical approximation

4. Conclusions

This paper presented two different CFD approaches to predict the tube-to-tube gap velocity distributions during sub-cooled feedwater (FW) blowdown caused by a FWLB using the real SG model containing tubes or the hollow SG model. It was shown that the predictions by both CFD approaches were in good agreement. To examine the validity of the CFD calculations, a simple analytical approximation was made for predicting the flow field under the conditions with known discharge flowrate at the FW nozzle exit applying a line sink model. The simple analysis confirmed the applicability of CFD simulations.

REFERENCES

[1] J.C. Jo and W.K. Shin, Fluidelastic Instability Analysis of Operating Nuclear Steam Generator U-Tubes, NED, Volume 193, Issue No.1-2, pp. 55-71, 1999.

[2] J.C. Jo, J.J. Jeong, and F.J. Moody, Transient Hydraulic Response of a Pressurized Water Reactor Steam Generator to a Feedwater Line Break Using the Nonflashing Liquid Flow Model, ASME JPVT, Vol. 139, pp. 031302-1~9, 2017.

[3] J.C. Jo, J.J. Jeong, B.J. Yun, and F.J. Moody, Numerical Prediction of a Flashing Flow of Saturated Water at High Pressure, NET Vol. 50, pp. 1173-1183, 2018.

[4] J.C. Jo, J.J. Jeong, B.J. Yun, and J. Kim, Numerical Analysis of Sub-Cooled Water Flashing Flow from a Pressurized Water Reactor Steam Generator through an Abruptly Broken Main Feed Water Pipe, ASME JPVT, in print, 2019.

[5] F.R. Menter, Two Equation Eddy-Viscosity Turbulence Models for Engineering Applications, AIAA J., Vo. 32, No. 8, pp. 1598-1604, 1994.

[6] ANSYS CFX User's Guide-19, New York, 2018.

[7] R.D. Blevins, Applied Fluid Dynamics Handbook, Krieger, 2003.

[8] D. Lasseux, F.J. Valdés-Parada, On the Developments of Darcy's Law to Include Inertial and Slip Effects, Comptes Rendus Mecanique, 2017.

[9] H.R. Vallentine, Applied Hydrodynamics, London Butterworths, 1959.